Twenty-Seventh Symposium (International) on Combustion/The Combustion Institute, 1998/pp. 625–632

AN EXPERIMENTAL AND NUMERICAL INVESTIGATION OF THE STRUCTURE OF STEADY TWO-DIMENSIONAL PARTIALLY PREMIXED METHANE-AIR FLAMES

ZHUANG SHU, BRADY J. KRASS, CHUN W. CHOI, SURESH K. AGGARWAL, VISWANATH R. KATTA* AND ISHWAR K. PURI

Department of Mechanical Engineering (M/C 251)
University of Illinois at Chicago
842 W. Taylor St., RM 2039
Chicago, IL 60607-7022, USA

Steady two-dimensional partially premixed slot-burner flames established by introducing a rich fuel-air mixture from the inner slot and air from the two outer slots are investigated. Numerical simulations are conducted using detailed chemistry, velocity measurements are made using particle image velocimetry, and images of the chemiluminescent reaction zones are obtained. Two reaction zones are evident; one in an inner rich-side premixedlike flame and the other in an outer lean-side non-premixed flame. Validation of the predictions involves a comparison of the (1) premixed and non-premixed flame heights, (2) the double-flame structure, and (3) velocity vectors. The measured and predicted velocity vectors are in good agreement and show that the flame interface separates smaller velocity magnitudes on the reactant side from larger values on the (partially) burned side. The outer flame temperature is higher than that of the inner premixed flame. A substantial amount of methane leaks past the inner flame and reacts in the outer non-premixed zone. The inner flame produces partially oxidized products such as H_2 and CO, which provide the fuel for the non-premixed flame. The initiation reaction $CH_4 + H \Leftrightarrow CH_3 + H_2$ proceeds strongly at the base of the flame where both the inner and outer flames are connected and at the tip of the inner flame, and it is weak along the sides of both inner and outer flames in accord with the chemiluminescent images. Carbon dioxide formation through the reaction $CO + OH \Leftrightarrow CO_2 + H$ is more diffuse than methane consumption in the outer flame, because the availability of hydroxyl radicals in that region is limited through oxidizer transport.

Introduction

Partially premixed flames are established when a fuel-rich mixture is separated from a fuel-lean mixture by the flame, and both fuel and oxidizer are simultaneously present on at least one side of the flame interface. A generic partially premixed flame consists of two streams with, respectively, rich and lean side equivalence ratios ϕ_r and ϕ_1, where $1 < \phi_r \leq \infty$ and $0 \leq \phi_1 < 1$ [1]. Partially premixed flames may also occur in those regions of non-premixed flames where fuel-air mixing ensues as a consequence of local quenching (e.g., during flame liftoff) and in premixed applications due to poor initial mixing. For instance, Rogg et al. [2] have observed that partial premixing of laminar flamelets is essential for the prediction of non-premixed turbulent flame structure. In spray flames, nonuniform evaporation can result in locally fuel-rich regions in which burning occurs in the partially premixed mode.

Previous investigations of partially premixed flames have employed counterflow and coflow flame configurations [2–11]. Yamaoka and Tsuji [3–5] have investigated partially premixed flames established in the forward stagnation region of a porous cylinder that was immersed in a uniform air stream and observed that, depending on the stoichiometry of the premixed mixture, two separate reaction zones could be established. Opposed-jet counterflow flame studies have shown partial premixing to make the flames less resistant to stretch under certain circumstances and for these flames to exhibit both a diffusion and premixedlike structure [6–8]. More recent investigations have focused on unsteady flames [9–11]. The objective of this investigation is to (1) investigate the flame structure of two-dimensional partially premixed flames in greater detail and (2) provide experimental validation for our numerical model.

Procedure

Numerical Method

A time-dependent two-dimensional model based on a direct numerical simulation methodology is

*Present address: Innovative Scientific Solutions, Inc. Dayton, OH 45430.

employed, and a relatively detailed 17-species, 52-step mechanism proposed by Peters [12] is used to represent the CH_4-air chemistry. The governing equations can be written in Cartesian coordinates (x, y) in the form

$$\frac{\partial(\rho\phi)}{\partial t} + \frac{\partial(\rho u\phi)}{\partial x} + \frac{\partial(\rho v\phi)}{\partial y} = \frac{\partial}{\partial x}\left(\Gamma^{\phi}\frac{\partial\phi}{\partial x}\right) + \frac{\partial}{\partial y}\left(\Gamma^{\phi}\frac{\partial\phi}{\partial y}\right) + S^{\phi}$$

where ρ represents the density and u and v the transverse (x) and axial (y) velocity components, respectively. The general form of the foregoing equation represents either of the mass, momentum, species, or energy conservation equations. The transport coefficient Γ^{ϕ} and the source terms S^{ϕ} appearing in the governing equations are provided in Ref. [10]. Using the overall species conservation equation and the equation of state completes the set of governing equations. A detailed algorithm, similar to that in CHEMKIN [13], is employed to calculate the thermodynamic and transport properties. The equations are integrated by using a finite-control volume approach with a staggered, nonuniform grid system. The finite-difference forms of the momentum equations are obtained using an implicit scheme [14], while those of the species and energy equations are obtained using a hybrid scheme [15]. Further details about the numerical procedure, validation, and the treatment of boundary conditions are provided in earlier publications [10,11,16–19].

Experimental Method

Instantaneous measurements of the velocity vectors and the flame heat release are made. We have used instruments that can be readily used to characterize analogous unsteady flames that are to be the focus of a subsequent investigation.

Particle image velocimetry

Particle image velocimetry (PIV) is a useful method to gain quantitative instantaneous information about an unsteady flow field. Using this technique, a portion of the flow field is illuminated, and the Lorenz–Mie scattering from seed particles is imaged. Although the technique is valuable, implementing it in reacting flows presents challenges due to the large range of particle seeding densities that are required due to flow dilatation [20] so that only a few applications to combustion systems have been reported [21–28], none for partially premixed flames.

The particle illumination source consists of a double-pulsed Continuum Nd:YAG laser, and the flow is seeded with TiO_2 particles. Particle images are captured two times (due to the double pulse) using a TI RS-170 CCD camera. The digitized image is fed to an array processor and analyzed using commercial autocorrelation software obtained from TSI. The analysis involves dividing the image into a grid and taking a two-dimensional fast Fourier transform (FFT) of the sections to determine the peak intensity locations. The distances between those locations are measured, and a velocity vector is predicted. Several precautions are taken to ensure reliability. Each interrogation spot contains more than 10 particle image pairs. Through extensive trial and error, the interrogation spot size is made small enough for a single vector to describe the flow at that location, and the laser sheet is made thick enough for out-of-plane particle motion to not be problematic and for sufficient particle pairs to be present. The particle displacement is kept greater than two particle image diameters but not more than one-quarter of the interrogation spot size. The overlap between spots is adjusted to increase the vector density. Further details of the PIV system are contained in Ref. [29].

C_2-radical imaging

In general, the chemiluminescent emission from flames may be interpreted as a signature of chemical reaction and heat release from which the flame geometry can be determined [30–33]. The excited states of CH and OH have been, respectively, suggested as the major emitters from the premixed and non-premixed reaction zones of partially premixed flames [34]. The excited C_2^* free radical species is short-lived and is also a good indicator of the reaction zone [32], and its light intensity is known to vary linearly with the volumetric heat release [33]. Spectral emission images are obtained at the 473-nm wavelength (1,0) C_2 Swan band [35]. We have used an ITT F4577 513 × 480 pixel intensified camera and a narrow wavelength interference filter (470 ± 10 nm). The spectral response of the CCD camera is relatively flat in the range between 420 and 900 nm and is ≈0.02 amps/W at 470 nm. The images are transferred to a frame grabber (P360F, Dipix) and processed after subtracting a representative background image to obtain a histogram that consists of a matrix in which each pixel gray level is represented by an integer N in the range $0 \leq N \leq 256$.

Configuration

The flames are established on a rectangular Wolfhard–Parker slot burner, a schematic diagram of which is shown in Fig. 1. A rich fuel-air mixture is introduced from the inner slot and air from the two outer slots. The aspect ratio of the inner slot is 5.6, and the three-slot burner establishes a flame with two identical two-dimensional flame sheets [36]. In such a rectangular geometry, where cross-stream line-of-sight integration may be acceptable, emission measurements provide an inexpensive alternative to more sophisticated laser-based methods. The

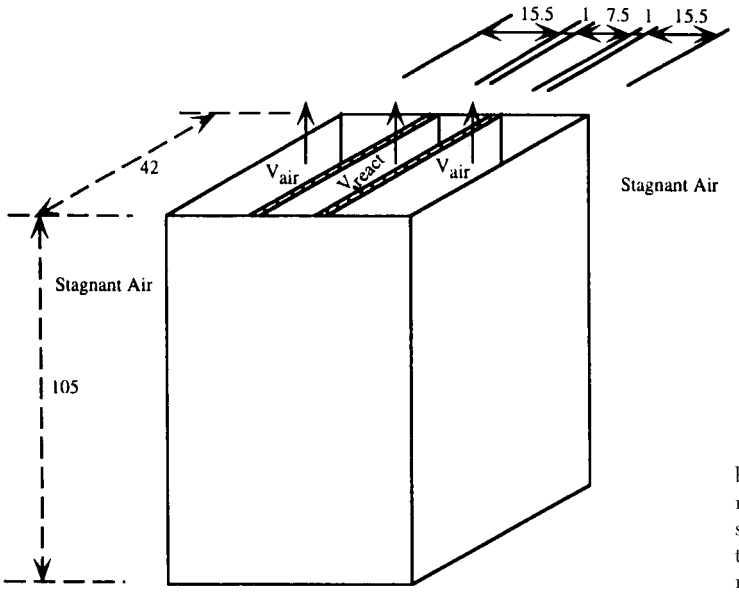

FIG. 1. Schematic diagram of the burner that consists of an inner 7.5-mm slot with two 15.5-mm outer slots on either side of it. The wall thickness separating the slots is 1 mm. Ceramic flow straighteners are placed in all three slots.

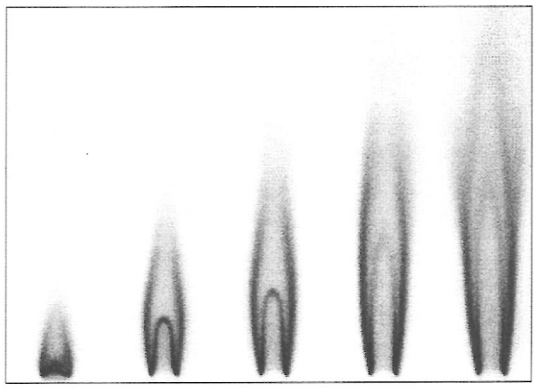

FIG. 2. C_2-emission images from flames established at $\phi = 2$, $V_{air} = 30$ cm s^{-1}, and (successively from left to right) $V_{reac} = 20$, 30, 40, 50, and 70 cm s^{-1}.

numerical simulations are conducted on one side of the symmetry plane of a two-dimensional domain. The other planes bounding the domain consist of two free surfaces and the inlet plane.

Results and Discussion

In the experiments, methane-air mixtures are introduced through the inner slot at fuel-rich equivalence ratios $\phi = 2$, 2.5, and 3. For each of these conditions, the inner and outer slot velocities (respectively, V_{reac} and V_{air}) are varied such that $V_{reac} = 20$, 30, 40, 50, and 70 cm s^{-1}, and $V_{air} = 30$, 50, and 70 cm s^{-1}. Figure 2 contains a representative set of C_2^*-emission images for flames established at fixed values of ϕ and V_{air} but at the five reactant flow velocities. Two distinct reaction zones are evident, one each on the rich and lean sides of the flow. The flames exhibit a double-flame structure over the range of flow rates investigated. In analogous counterflow flames established at this stoichiometry, the two flames were found to be merged [37], although it is known that the double-flame structure exists at low-enough flame stretch rates [34]. This indicates that the slot burner flame adjusts to locations where the fuel-side stretch rates are low and exhibits a double-flame structure.

Both the inner and outer flame heights grow as the reactant velocity (and, thereby, reactant flux) increases. The two flame heights also increase as the equivalence ratio is raised, because the stoichiometry moves from a premixedlike mode ($\phi \to 1$) to a non-premixed condition ($\phi \to \infty$) so that the flame

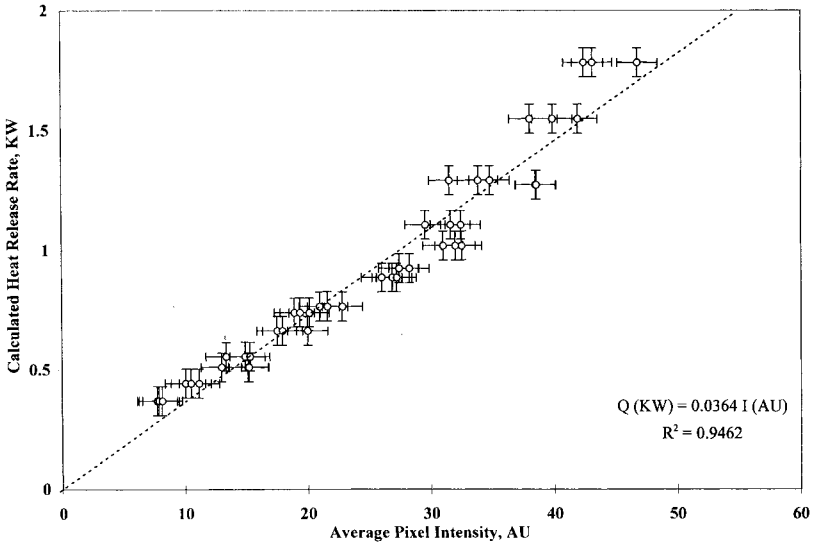

FIG. 3. Correlation of the predicted heat-release rate Q based on the measured flow rates with the average pixel C_2-chemiluminescence intensity I. The linear relationship is of the form $Q = 0.036I$. Bars represent the standard error.

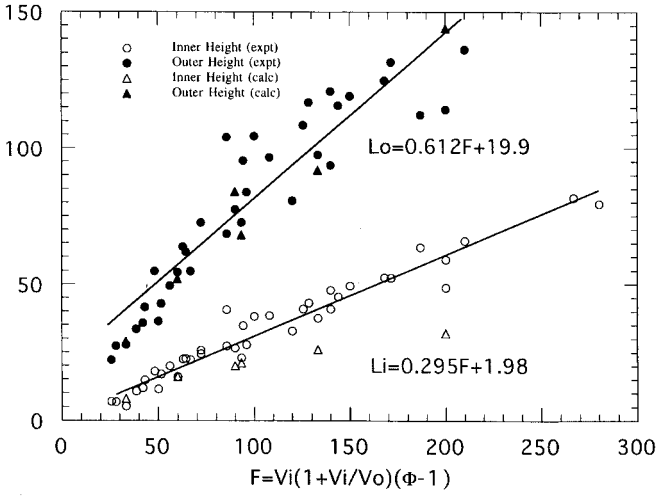

FIG. 4. Correlation of the inner (L_i) and outer (L_0) flame heights with the function $V_{reac}(1 + V_{reac}/V_{air})(\phi - 1)$. The closed and open symbols, respectively, denote the outer and inner flame heights. The circles and triangles (● and ▲), respectively, represent the measured and predicted values. Six flame heights are predicted for the conditions $\phi = 2$, $V_{reac} = 20$, 30, 40, and 50 cm s^{-1}, $V_{air} = 30$ cm s^{-1}; and $\phi = 2.5$, $V_{reac} = 30$ and 50 cm s^{-1}, $V_{air} = 30$ cm s^{-1}.

becomes mixing limited. Increasing the outer velocity decreases both flame heights because the higher air-side flux reduces the outer (non-premixed-type) flame height, which, in turn, interacts with the inner (premixedlike) flame whose height also declines.

The C_2^* emission signal is confined to relatively thin sheetlike reaction zones. For that reason, the total signal is directly proportional to the flame surface area and is well correlated with the reactant flow rate in accord with previously reported results [33,38]. Figure 3 contains a plot of the average pixel intensity I with respect to the predicted heat-release rate Q based on the reactant flow rate in the form of a linear relationship $Q = \alpha I$. The chemiluminescence images are directly proportional to the C_2^* formation rate and, thus, serve as a qualitative rate measure of the flame chemistry [39].

Figure 4 contains a correlation of both flame heights with the function $F = V_{reac}(1 + V_{reac}/V_{air})(\phi - 1)$. The measured outer flame height L_0 data show greater scatter than the corresponding inner flame heights L_i. While measurements of L_i are straightforward, the outer flame emission provides images consisting of two unclosed interfaces on either side of the inner slot. Geometric tangents must be superimposed upon these interfaces in order to

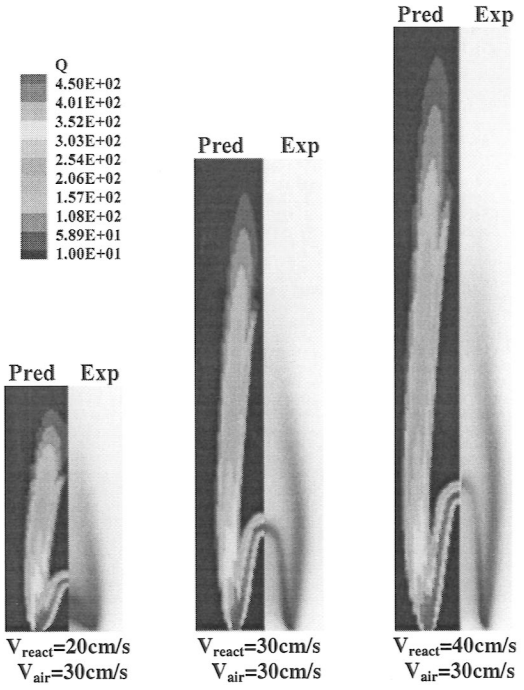

FIG. 5. Comparison of the simulated heat-release rates with the experimentally obtained C_2-chemiluminescence images for three flames established at $\phi = 2$ and $V_{air} = 30$ cm s^{-1}, and with $V_{reac} = 20$, 30, and 40 cm s^{-1}.

evaluate L_0, leaving its exact value open to some interpretation. Furthermore, at higher V_{reac} values, the outer flames become unsteady and begin to slowly flicker. Consequently, the outer images become somewhat thicker and more diffuse, introducing additional error into the tangent measurements, particularly as ϕ increases. Therefore, some L_0 values are not reported. Regardless of these uncertainties, the inner and outer flame heights are well correlated with F. A linear best fit provides relations for the inner flame height $L_i = (0.3F + 2)$ mm, and the outer height $L_0 = (0.6F + 20)$ mm in the ranges $25 \leq F \leq 280$ mm, $5 \leq L_i \leq 85$ mm, and $20 \leq L_i \leq 145$ mm.

While there is excellent agreement between the measured and predicted values of L_0, a comparison of the corresponding inner flame heights shows a progressively larger disagreement as F increases. Najm et al. [39] have suggested that the largest share of the carbon flow in methane-air flames is carried by the path $CH_3 \rightarrow CH_2O \rightarrow CHO \rightarrow CO$ (initiated by the reaction $CH_3 + O \Leftrightarrow CH_2O + H$), and only a minor amount by reactions involving the methyl radical that finally produce excited-state C_2. The predicted flame heights contained in Fig. 4 are based on the two peak axial centerline values of the initiation reaction $CH_4 + H \Leftrightarrow CH_3 + H_2$, corresponding to the inner and outer flames. Our analysis has shown that the simulated flame heights based on this criteria are virtually identical to those based on the peak heat-release rates; the peak rates of $CH_3 + O \Leftrightarrow CH_2O + H$; the peak CO-formation rates through the reaction $CHO + M \Leftrightarrow CO + H + M$; and either the peak formyl radical mole fractions or the peak CHO formation rates (as CHO has been reported to be an excellent marker of flame heat release [39]). Therefore, the discrepancy between the predicted and measured values of L_i is not due to a spatial difference between the predicted heat release and measured C_2^*-emission regions and must be attributed to the rich-side flame chemistry. This will be the focus of a subsequent investigation.

Figure 5 presents a comparison of the predicted heat-release rates with the experimentally obtained emission images for four flames. The comparison is less satisfactory when V_{reac} is smaller. This may be attributed to the proportionally larger heat losses (which are not simulated) from the smaller flame to the burner during the experiments. These losses influence the inner premixedlike reaction zone more than the outer transport-limited non-premixed reaction region. There is good agreement when the air and reactant velocities are identical, and the comparison again exhibits some discrepancies when V_{reac} exceeds V_{air}. Some differences are to be expected (particularly on the rich side and, consequently, related to the inner flame heights), because C_2 chemistry is neglected in the simulations. However, even when a quantitative comparison fails, it is possible to accurately simulate the qualitative shape and structure of the reaction zone.

The emission signal is strongest at the base of the

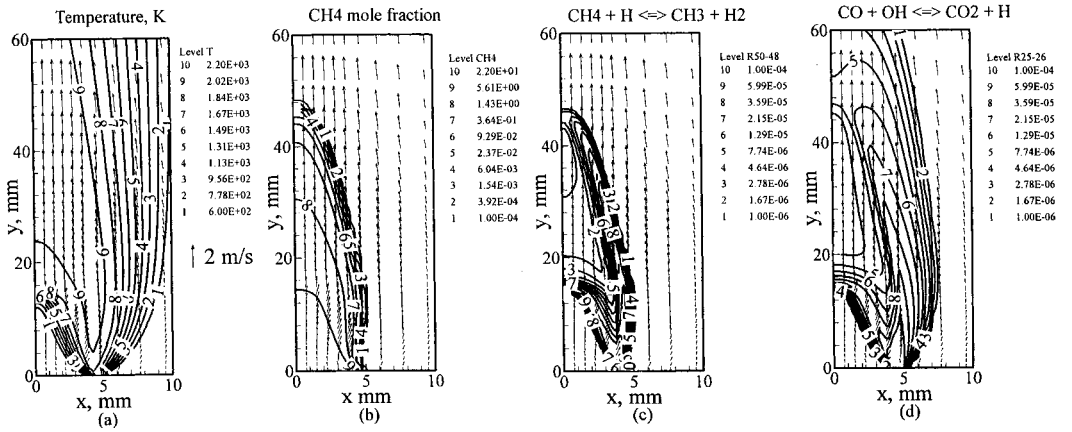

FIG. 6. (a) Comparison of the measured ($-4 \leq x \leq 0$ mm) and predicted velocity vectors ($0 \leq x \leq 4$ mm) for a flame established at $\phi = 2$, $V_{air} = 30$ cm s^{-1}, and $V_{reac} = 30$ cm s^{-1}. The corresponding flame interface (chemiluminescent image and simulated heat release) are superimposed on the two plots. (b) Comparison of the measured (●) and predicted (○) centerline velocities for a flame established at $\phi = 2$, $V_{air} = 30$ cm s^{-1}, and $V_{reac} = 30$ cm s^{-1}.

inner and outer flames, that is, where the two flames are connected. Both the simulated heat-release rates and the chemiluminescence along the sides of the inner (premixed) flame decrease due to stretch effects as V_{reac} increases, with higher levels being associated with the flame tip and base. Therefore, it appears that the reaction zone is more vigorous at the tip and base of the inner flame than along its sides. The heat-release rate progressively decreases along the outer (non-premixed) flame at downstream locations. The non-premixed reaction zone has a weak tip, and reaction rates are stronger in upstream regions of that flame.

The measured and predicted velocity vectors are compared in Fig. 6a. The measurements mirror the simulations, and the flame interface separates smaller velocity magnitudes on the reactant side from larger values on the (partially) burned side. Both sets capture the air entrainment in the region between $3 \leq x \leq 1.5$ mm and $0 \leq y \leq 4$ mm where the velocity vectors turn toward the centerline. The gas expansion due to heat release causes the velocity vectors to move outward with respect to the centerline along the inner flame.

In order to obtain accurate data for the range of flow velocities, the PIV measurement window was set at 7.5×5.5 mm, respectively, in the x- and y-wise directions. This choice restricted the lowest possible velocity measurement for the acquired particle displacements to 30 cm s^{-1} (which equals the reactant and air inlet velocities). The experimental data are sparse in some postflame regions, because flow dilatation greatly reduces the particle seed densities in those areas. Although the measured velocities were obtained after averaging the vectors acquired from 10 PIV images, they are representative of each of those images. The measured and predicted velocities along the flame centerline (which, being in the symmetry plane, contain only an axial component) are compared in Fig. 6b. There is good agreement between the two sets in the preflame zone, but there is some discrepancy in the postflame region that is probably due to experimental uncertainties. The centerline velocity profile is representative of a preflame preheat zone, the inner (premixed) flame zone, and a postflame zone that is heated due to heat transfer from the outer flame.

These zones can be differentiated in the flame structure presented in Fig. 7 (for a flame exhibiting excellent agreement between the experiments and predictions). The region between the inner and outer flames is the hottest as seen from the temperature contours of Fig. 7a. The outer reaction zone temperature is higher than that of the inner premixed flame. A substantial amount of methane leaks past the inner flame and reacts in the outer non-premixed zone, as presented in Fig. 7b. Likewise, oxygen is consumed in both the inner and outer flames. Oxygen is entrained into the outer non-premixed flame, as can be seen by examining the air-side velocity vectors, which advect air to the centerline. The inner flame produces partially oxidized products, such as H_2 and CO that provide the "fuel" for the non-premixed flame. The velocity vectors turn toward the outer slots in the post-inner flame region, thereby advecting these species into the non-premixed flame.

The initiation reaction $CH_4 + H \Leftrightarrow CH_3 + H_2$ proceeds strongly at the base of the flame, where both the inner and outer flames are connected, and at the tip of the inner flame. On the other hand, it is weak along the sides of the inner and outer flames.

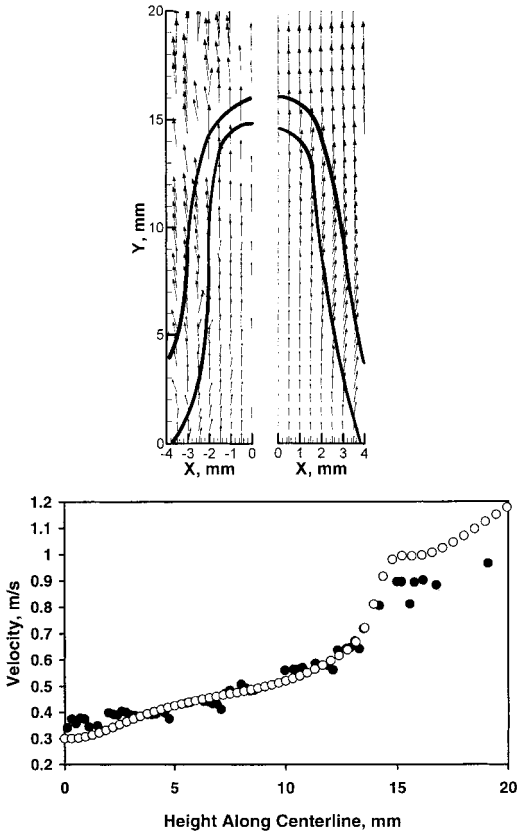

FIG. 7. Predicted flame structure of a flame established at $\phi = 2$, $V_{air} = 30$ cm s^{-1}, and $V_{reac} = 30$ cm s^{-1}. (a) Temperature, (b) CH_4 mole fraction, (c) the rate of the reaction $CH_4 + H \Leftrightarrow CH_3 + H_2$, and (d) the rate of the reaction $CO + OH \Leftrightarrow CO_2 + H$.

This is in accord with the chemiluminescent images contained in Fig. 2 that show that while the outer flame tip is open, the inner flame is always closed for the investigated range of conditions. The CO-oxidation reaction $CO + OH \Leftrightarrow CO_2 + H$ shown in Fig. 7d exhibits a similar distribution. Carbon dioxide formation through this reaction is more diffuse in the outer flame, because the availability of hydroxyl radicals in that region (through the initiation step $O_2 + H \Leftrightarrow OH + O$) is limited by oxidizer transport.

Conclusions

The results of an experimental and numerical investigation of two-dimensional partially premixed methane-air flames are presented. A detailed validation of the predictions involves a comparison of the (1) inner and outer flame heights over a wide range of conditions, (2) flame reaction zones, and (3) velocity vectors. Overall, the comparison is excellent, but some discrepancies remain. Some are likely due to the absence of C_2 chemistry in the simulations. This aspect will be explored in future work.

1. For the range of conditions considered, sheetlike inner (premixed) and outer (non-premixed) reaction zones are formed. The inner (premixed) flame zone has a closed tip, and reactions proceed stronger at its base and tip than along its sides. The flames exhibit a double-flame structure over the range of investigated flow rates, indicating that the flame location self-adjusts itself to locations where the fuel-side stretch rates are low.
2. The measured and predicted values of L_0 are in good agreement. Comparisons of the corresponding values of L_i show a progressively larger disagreement as F increases, which is attributed to the rich-side flame chemistry, because C_2 chemistry is neglected in the simulations. Both flame heights correlate well with the function $F = V_{reac}(1 + V_{reac}/V_{air})(\phi - 1)$.
3. The flame has four zones: an inner preflame preheat zone, the inner (premixed) flame zone in which CO and H_2 are formed, a post-inner flame zone situated between the inner and outer flames containing hot products, and a non-premixed outer region in which CO and H_2 oxidation occur.

Acknowledgments

This research was supported by the National Science Foundation Combustion and Plasma Systems Program through Grant Number CTS-9707000 for which Dr. Farley Fisher is the Program Director. We are grateful to Dr. Anthony Hamins (NIST) for sharing a slot burner design.

REFERENCES

1. Seshadri, K., Puri, I., and Peters, N., *Combust. Flame* 61:237–249 (1985).
2. Rogg, B., Behrendt, F., and Warnatz, J., in *Twenty-First Symposium (International) on Combustion,* The Combustion Institute, Pittsburgh, 1986, p. 1533.
3. Yamaoka, I. and Tsuji, H., in *Fifteenth Symposium (International) on Combustion,* The Combustion Institute, Pittsburgh, 1974, p. 737.
4. Yamaoka, I. and Tsuji, H., in *Sixteenth Symposium (International) on Combustion,* The Combustion Institute, Pittsburgh, 1976, p. 1145.
5. Yamaoka, I. and Tsuji, H., in *Seventeenth Symposium (International) on Combustion,* The Combustion Institute, Pittsburgh, 1978, p. 843.
6. Hamins, A., Thridandam, H., and Seshadri, K., *Chem. Eng. Sci.* 40:2027–2038 (1985).
7. Smooke, M. D., Seshadri, K., and Puri, I. K., in *Twenty-Second Symposium (International) on Combustion,* The Combustion Institute, Pittsburgh, 1988, pp. 1555–1563.

8. Law, C. K., Li, T. X., Chung, S. H., Kim, J. S., and Zhu, D. L., *Combust. Sci. Technol.* 64:199–232 (1989).
9. Brown, T. M., Pitz, R. J., and Sung, S. J., Paper no. AIAA 97-0903 presented at the AIAA 35th Aerospace Sciences Meeting and Exhibit, Reno, Nevada, January 6–10, 1997.
10. Shu, Z., Aggarwal, S. K., Katta, V. R., and Puri, I. K., *Combust. Flame* 111:276–295 (1997).
11. Shu, Z., Aggarwal, S. K., Katta, V. R., and Puri, I. K., *Combust. Flame* 111:296–311 (1997).
12. Peters, N., in *Reduced Kinetic Mechanisms for Applications in Combustion Systems, Lecture Notes in Physics* (N. Peters and B. Rogg, eds.), Springer-Verlag, New York, 1996, vol. m15, pp. 3–14.
13. Kee, R. J., Miller, J. A., and Warnatz, J., "A Fortran Program Package for the Evaluation of Gas-phase Viscosities, Conductivities, and Diffusion Coefficients," Sandia National Laboratories report SAND83-8209.
14. Leonard, B. P., *Comput: Meth. Appl. Mech. Eng.* 19:59–98 (1979).
15. Spalding, D. B., *Int. J. Num. Meth. Mech. Eng.* 4:551 (1972).
16. Katta, V. R., Goss, L. P., and Roquemore, W. M., *Combust. Flame* 96:60–74 (1994).
17. Takahashi, F. and Katta, V. R., *AIAA J. Propul. Power* 11 (1995).
18. Aggarwal, S. K., Park, T. W., and Katta, V. R., *Combust. Sci. Technol.* 113:429–438 (1996).
19. Patadia, H., "Transient Structure of Methane-Air and Methanol-Air Diffusion Flames," Master's thesis, The University of Illinois at Chicago, 1995.
20. Frank, J. H., Lyons, K. M., and Long, M. B., *Combust. Flame* 107:1–12 (1996).
21. Reuss, D. L., Bardsley, M., Felton, P. G., Landreth, C. C., and Adrian, R. J., SAE paper 90-0053.
22. Armstrong, N. W. H., Ph.D. thesis, University of Cambridge, 1992.
23. Goss, L. P., Post, M. E., Trump, D. D., and Sarka, B., *J. Laser Appl.* 3:36–42 (1991).
24. Reuss, D. L., Landreth, C. C., and Adrian, R. J., *Combust. Sci. Technol.* 67:73–83 (1989).
25. Armstrong, N. W. H. and Bray, K. N. C., SAE paper 92-2322.
26. Lecordier, B., Mouquallid, S., Vottier, S., Rouland, E., Allano, D., and Trinite, M., *Exp. Fluids* 17:205–208 (1994).
27. Driscoll, J. F., Stukus, D. J., Roberts, W. L., Post, M. E., and Goss, L. P., *Combust. Sci. Technol.* 96:213–229 (1994).
28. Ereaut, P. R., *J. Inst. Energy* 62:14–20 (1989).
29. Bunnell, R. K., "A Theoretical and Experimental Investigation of Well-Mixed Combustion in a Rapid-Mixing Burner," Master's thesis, The University of Illinois at Chicago, 1996.
30. Beyler, C. L. and Gouldin, F. C., in *Eighteenth Symposium (International) on Combustion,* The Combustion Institute, Pittsburgh, 1981, pp. 1011–1019.
31. Dibble, R. W., Long, M. B., and Masri, A., *Prog. Astronaut. Aeronaut.* 105:99–109 (1986).
32. Brandon, Y. and Samaniego, J.-M., *Combust. Sci. Technol.* 84:81–89 (1992).
33. McManus, K., Yip, B., and Candel, S., *Exptl. Thermal Fluid Sci.* 10:486–502 (1995).
34. Nishioka, M., Nakagawa, S., Ishikawa, Y., and Takeno, T., *Combust. Flame* 98:127–138 (1994).
35. Pearse, R. W. B. and Gaydon, A. G., in *The Identification of Molecular Spectra,* 4th ed., Chapman and Hall, London, 1976, p. 83.
36. Smyth, K. C. and Tjossem, P. J. H., in *Twenty-Third Symposium (International) on Combustion,* The Combustion Institute, Pittsburgh, 1990, pp. 1829–1837.
37. Tanoff, M., Smooke, M. D., Osborne, R. J., Brown, T. M., and Pitz, R. W., in *Twenty-Sixth Symposium (International) on Combustion,* The Combustion Institute, Pittsburgh, 1996, pp. 1121–1128.
38. Hurle, I. R., Price, R. B., Sugden, T. M., Thomas, R. R. S., and Thomas, A., *Proc. R. Soc. London A* 303:409–427 (1968).
39. Najm, H. N., Paul, P. H., Mueller, C. J., and Wyckoff, P. S., *Combust. Flame* 113:312–332 (1998).